Available online at www.sciencedirect.com
ScienceDirect
Continental Shelf Research 27 (2007) 634–649
CONTINENTAL SHELF RESEARCH
www.elsevier.com/locate/csr

Temperature trends and interannual variability in the Strait of Georgia, British Columbia

Diane Masson*, Patrick F. Cummins

Institute of Ocean Sciences, Fisheries and Oceans Canada, P.O. Box 6000, 9860 W. Saanich Rd., Sidney, BC, Canada V8L 4B2

Received 19 May 2006; received in revised form 19 September 2006; accepted 24 October 2006
Available online 2 January 2007

Abstract

A continuous 36 year long record of semi-monthly temperature profiles from the central Strait of Georgia, British Columbia is used to examine low frequency variability and trends through the water column. Decomposition of temperature anomalies into empirical orthogonal functions shows that the dominant mode accounts for 78% of the variance, while the principal component associated with this mode (PC1) is dominated by fluctuations on interannual time scales. To relate the variability within the Strait to that occurring over the northeast Pacific, PC1 is compared with anomalies in local air temperature, sea surface temperatures off the west coast of Vancouver Island, and upper ocean temperatures along Line-P. These comparisons suggest that much of the interannual variability observed in the Strait of Georgia occurs in response to large-scale atmospheric forcing over the northeast Pacific. However, following tropical El Niño events there are significant anomalies associated with processes occurring along the coastal oceanic wave guide. The strongest event in the entire record, the remarkable negative temperature anomaly of winter 1978/1979, appears to be associated with a deep water intrusion that was forced locally.

A warming trend is observed over the period 1970–2005 through the entire water column of the Strait of Georgia, with a depth-averaged value of $0.024\,^{\circ}\mathrm{C\,yr^{-1}}$. The vertical variation of the linear trend in temperature is contrasted with trends observed through the upper water column in the adjoining northeast Pacific over the same time period. Comparable trends are observed within the upper 100 m of the water column. However, at greater depths trends in the Strait of Georgia exceed those observed offshore by a factor of two. This is likely a consequence of the entrainment of near-surface waters into the deep Strait by the estuarine circulation. The results illustrate how global climatic changes may be amplified at depth in a coastal sea.

Keywords: Temperature anomalies; Variability; Climatic changes; Estuarine circulation; El Niño phenomena; Northeast Pacific

1. Introduction

Data from tide gauges and lighthouses have typically formed the observational basis for the study of long term variability of British Columbia coastal waters. Continuous time series of sea surface temperature (SST) and salinity dating back to the first half of the 20th century are available from a number of such stations. Freeland (1990) examined the lighthouse data extant in 1989 and estimated SST trends along the coast. All stations, except for one with a very short record, displayed warming

*Corresponding author. Tel.: +1 250 363 6521; fax: +1 250 363 6746.
E-mail address: massond@dfo-mpo.gc.ca (D. Masson).

0278-4343/$ - see front matter © 2006 Elsevier Ltd. All rights reserved.
doi:10.1016/j.csr.2006.10.009

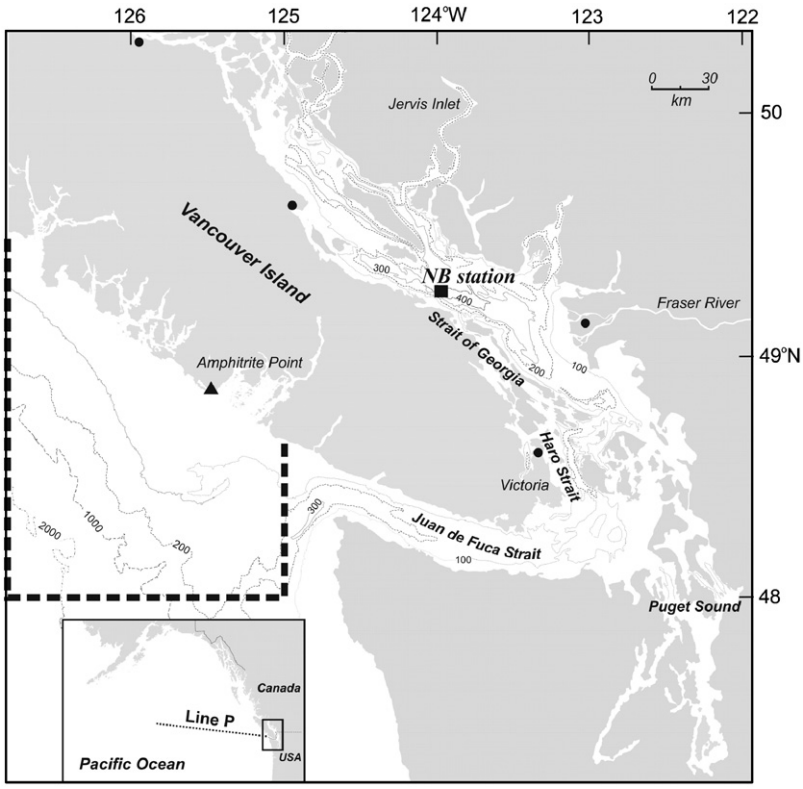

Fig. 1. Southern coastal British Columbia with locations of the Nanoose station (square), the Amphitrite Point lighthouse (triangle) and meteorological stations (circles) indicated. The dashed line shows the limits of the offshore region from which vertical temperature profiles were assembled. The dotted line in the inset indicates the location of the Line-P transect.

trends of varying magnitudes, depending on the length of the observational record. More recently, Gower (2002) made use of data from a network of meteorological buoys to estimate SST trends along the west coast of Canada and the United States.

In comparison to the surface data, there is a relative paucity of continuous time series for the subsurface water properties of coastal British Columbia. A notable exception is the repeat hydrographic profile data collected from a site, referred to herein as the Nanoose station,[1] whose location in the deep central Strait of Georgia is indicated in Fig. 1. While relatively long time series of subsurface data exist for open ocean locations in the northeast Pacific (e.g., Ocean Weather Station P; 145° W, 50° N), the Nanoose station is distinguished by virtue of its physical setting within a semi-enclosed basin that is dominated by a seasonally modulated estuarine circulation. This circulation is driven by a large freshwater discharge, mostly from the Fraser River, and is modulated by tidal mixing in the Haro Strait area and by local wind forcing (e.g., Waldichuk, 1957; LeBlond, 1983). Although time series of both temperature and salinity data are available from the Nanoose station, the focus in this paper is on the temperature data for which the observational record is both of longer duration and of generally higher quality. A continuous 36 year long record of semi-monthly temperature profiles is used to examine the low frequency variability and trends found through the water column in the Strait. The variability on annual and longer time scales in the deep waters of the Strait of Georgia has been considered previously by Pickard (1975) using time series of about 7 years duration.

Discussed below is the relationship between the trends and variability observed at the Nanoose station and the changes occurring offshore along the coast, and at larger scale in the adjoining waters of the northeast Pacific. For this purpose, we examine continuous time series of surface air temperature

[1]The station is within the Nanoose Bay Naval Underwater Weapons Test Range, located in the vicinity of Nanoose Bay, British Columbia.

from local meteorological stations and SST data collected at the Amphitrite Point lighthouse situated along the west coast of Vancouver Island (locations are given in Fig. 1). In addition, CTD and bottle cast data from an offshore region in proximity of Vancouver Island (Fig. 1) were averaged to produce a set of quarterly temperature profiles covering the same period as the Nanoose station data. Finally, use is also made of data from Line-P, an oceanographic section extending approximately 1400 km from Vancouver Island to Station P in the subarctic gyre of the North Pacific (see inset in Fig. 1).

2. Interannual and secular variations

Vertical profiles of temperature and salinity have been collected at the Nanoose station on average a few times a week since mid-1969 by the Department of National Defence of Canada. However, all the salinity observations prior to March, 1979 are suspect. Information on the instrumentation is provided in Appendix A. After a basic quality control to remove obvious outliers, the data were averaged into 3 m bins in the vertical and averaged in time to produce semi-monthly profiles of temperature and salinity. As the individual station profiles start at irregularly varying depth levels, observations from depths shallower than 3 m were not included and the uppermost depth of the binned data is 4.5 m. A climatological seasonal cycle was computed at each depth level and removed from the data. A 2.5-month boxcar filter was then applied twice to the residual to remove high frequency noise, thus defining the interannual anomalies.

Before examining the interannual variability, it is useful to review briefly details of the seasonal signal. Masson and Cummins (2004) have discussed recently the seasonal cycle of salinity in the Strait of Georgia. As is typical for temperate estuaries, the density field is controlled chiefly by salinity, and temperature is essentially a passive scalar. Fig. 2 shows the seasonal cycle of temperature, based on the semi-monthly data over the 36 year period 1970–2005. Also included in the figure are contours of the seasonal cycle of salinity at the Nanoose station, based on the shorter 1980–2005 period. The seasonally varying temperature indicates a clear division of the water column into a three-layer vertical structure. There is a near-surface layer that is directly influenced by the surface heat flux. Immediately below, centered at a depth of about 100 m, is a mid-depth layer that is marked by relatively cold (warm) intrusions in the spring (fall). These mid-depth seasonal maxima occur about 3 months after those seen at the surface. Finally, there is a deep layer for which the seasonal temperature range is of order 0.5 °C, with slightly colder (warmer) water in the summer (winter) months.

The characteristic three-layer vertical structure found in the central Strait of Georgia is a consequence of mid-depth intrusions that form in a region of strong mixing in Haro Strait and flow

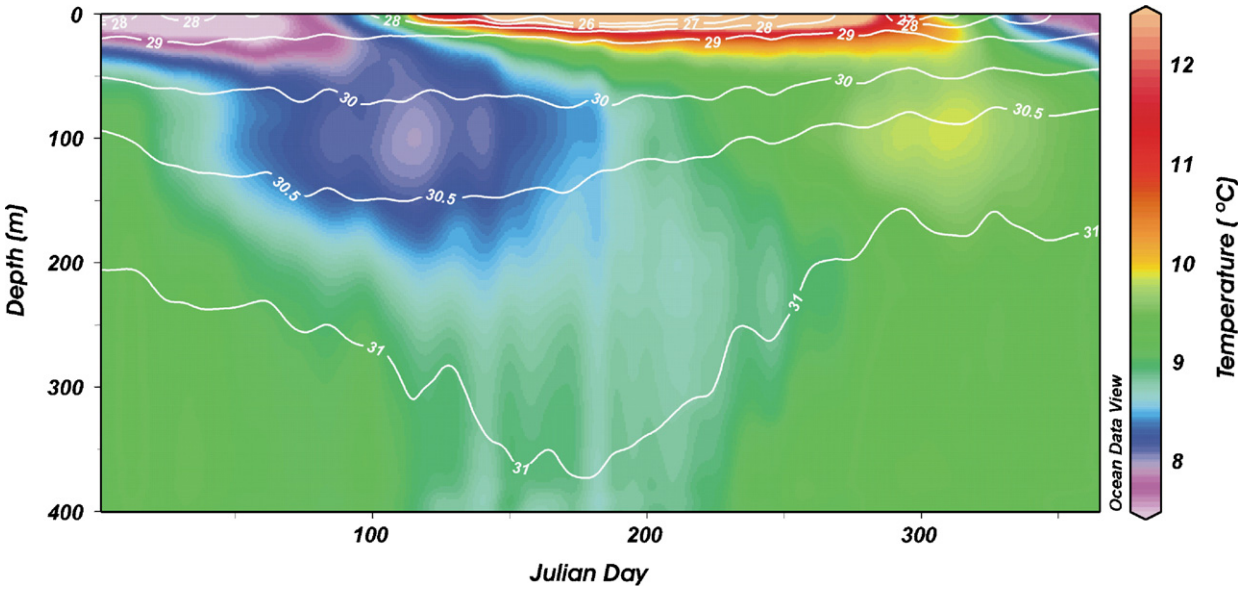

Fig. 2. Climatological seasonal cycle of temperature at the Nanoose station with contours of salinity superposed.

over the sill at Boundary Pass which separates Haro Strait and the Strait of Georgia (Fig. 1). These intrusions enter the Strait at approximately sill depth (100 m) and have a signature in various water properties. For example, Fig. 3 shows the concentration of dissolved oxygen measured at a series of 22 stations along the main axis of the estuary during a survey conducted in April, 2000. A detailed analysis of the water masses of Juan de Fuca Strait and the Strait of Georgia shows that the intrusions are composed of a mixture of water from the outflowing surface layer and water from the deep inflow into Juan de Fuca Strait that originates from the shelf (Masson, 2006). In the spring, intense tidal mixing in Haro Strait entrains relatively low temperature, oxygen-rich water from the surface which then penetrates into the central strait. During the fall season the intrusions are warm with respect to the ambient water (Fig. 2).

The interannual anomalies of temperature in the central Strait are illustrated in Fig. 4a and several significant features can be identified readily. Particularly striking are the pronounced warm and cool episodes which are manifested typically through most of the water column. This includes the positive anomalies of 1983, 1992 and 1998 that reflect the influence of El Niño events in the tropical Pacific, as well as negative anomalies in 1989 and 1999 associated with La Niña events. In contrast, a strong negative anomaly occurred in 1978/1979, but this event was found below a depth of 100 m with little surface signature. Fig. 4a also indicates the occurrence of a general warming trend throughout the entire water column. For comparison, the anomalies with the least squares fitted linear trend removed are presented in Fig. 4b and show more distinctly the interannual variability. (The depth-varying linear trends are discussed below in Section 2.1.)

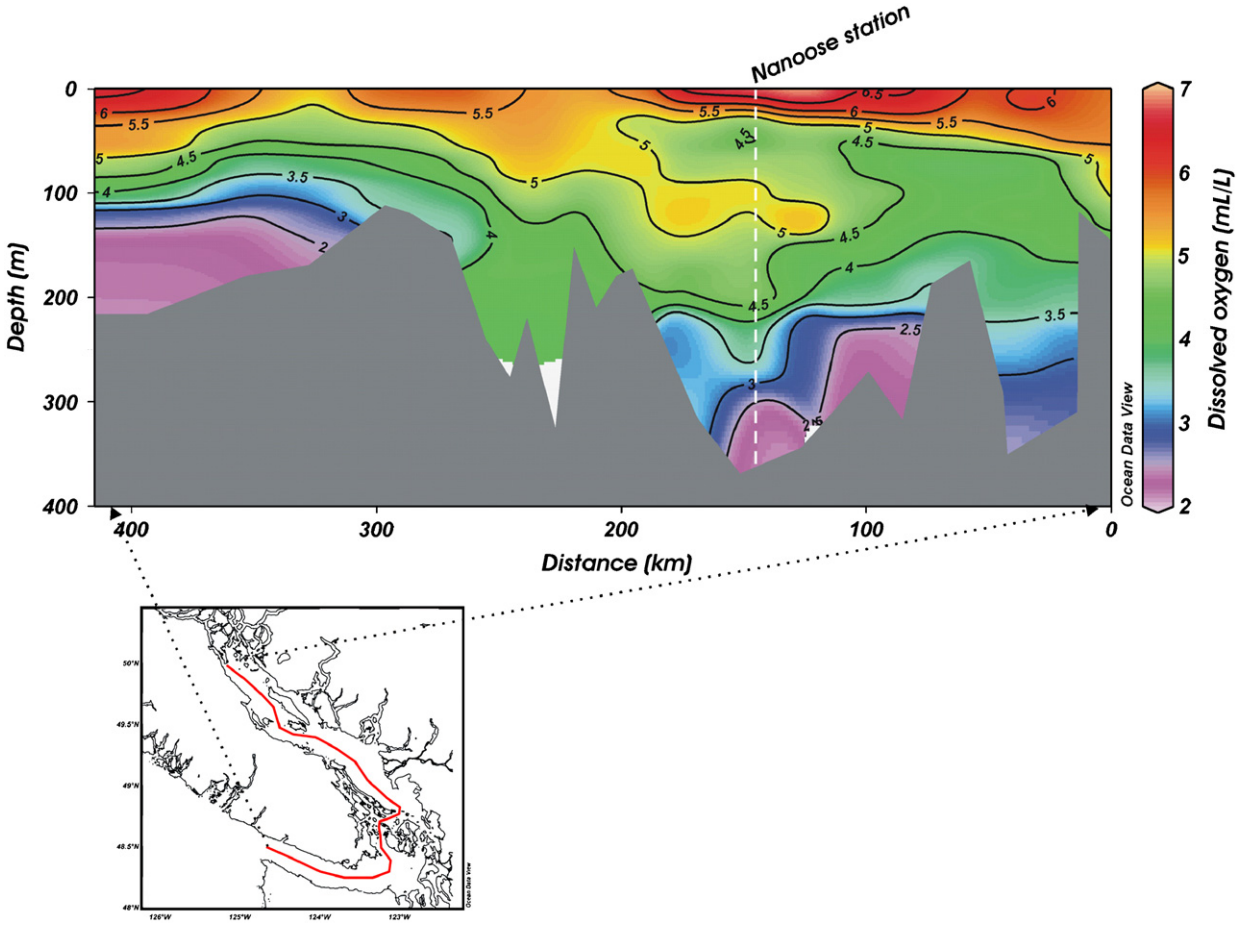

Fig. 3. Dissolved oxygen concentrations measured along the main axis of the coastal basin, during a seasonal survey in April, 2000. The position of the Nanoose station along the section is indicated.

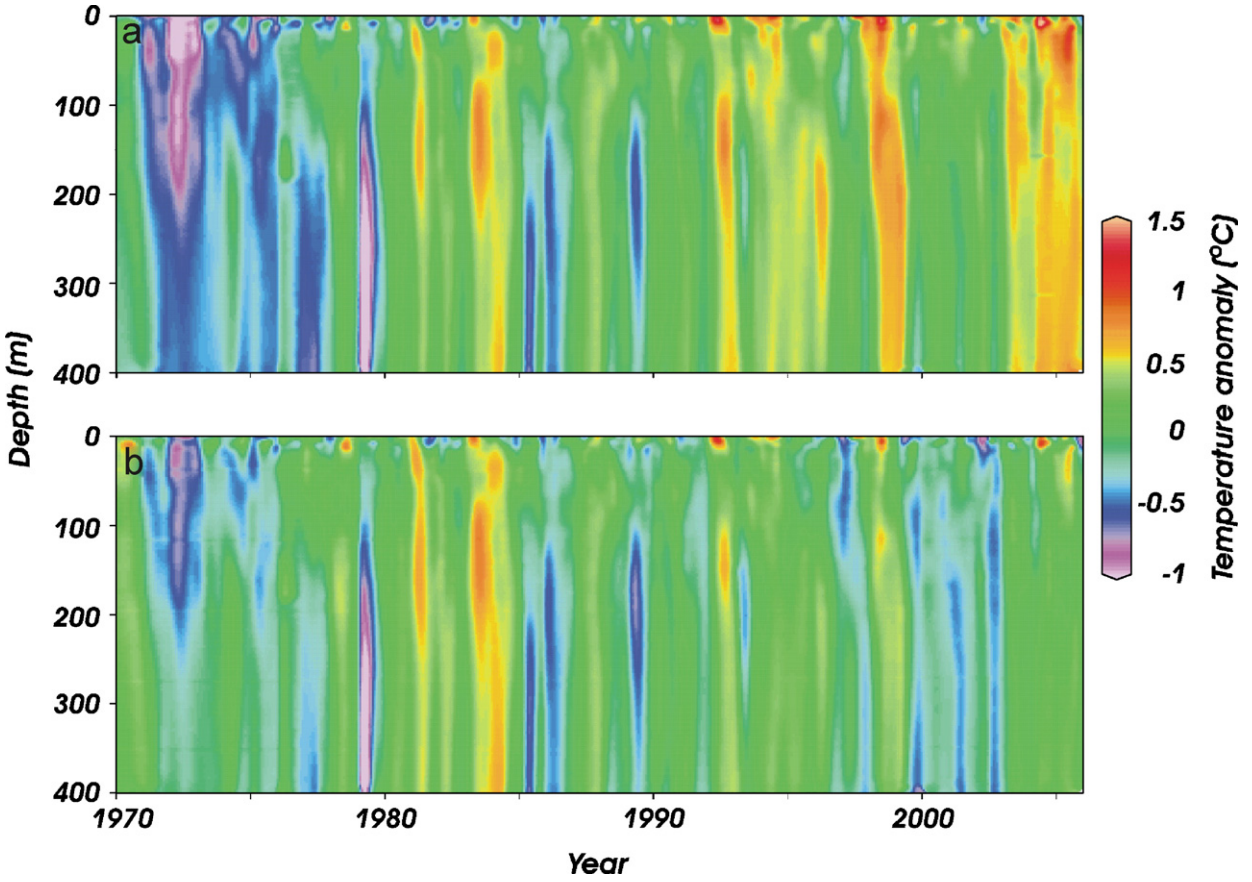

Fig. 4. (a) Temperature anomalies measured at the Nanoose station, and (b) the anomalies with the secular trend removed at each depth level.

A decorrelation time scale for the detrended anomalies was determined by fitting, in a least square sense, the autocorrelation function of a first-order autoregressive process, $\rho(k) = \alpha_1^{|k|}$, to the autocorrelation of the detrended anomalies. Here, k is the lag index and α_1 is the lag-1 correlation coefficient. The fit was carried out to lags of 2 years, although the results change only slightly if the maximum lag is increased to 4 years. The decorrelation time scale is then given by

$$\tau_d = \Delta t \sum_{k=-\infty}^{k=\infty} \rho(k) = \Delta t \frac{(1+\alpha_1)}{(1-\alpha_1)}, \quad (1)$$

where $\Delta t = \frac{1}{24}$yr is the time increment (von Storch and Zwiers, 1999).

The resulting values of τ_d are given in Fig. 5a and show an appreciable variation over the upper 100 m of the water column. There is a relatively short time scale for the layer closest to the surface, reflecting presumably the direct influence of short time scale atmospheric forcing. The decorrelation time scale reaches a maximum of 1.5 years around 60 m depth and then decreases to a fairly uniform intermediate value of about 1 year below 100 m depth. Thus, the longest time scales occur between the surface layer that is immediately influenced by atmospheric forcing and the layer of the sill depth intrusions. The variations seen in the decorrelation time scale suggest that distinct physical mechanisms account for the anomalies observed at different depths. In particular, the decrease of τ_d below its maximum at 60 m depth indicates a more direct connection with the surface layer through the advection of anomalies by intrusions from the sill region into the mid-depth and deep layers. This is consistent with Pickard (1975) who contended that changes occurring below 100 m depth are due to lateral advection rather than to local vertical transfers.

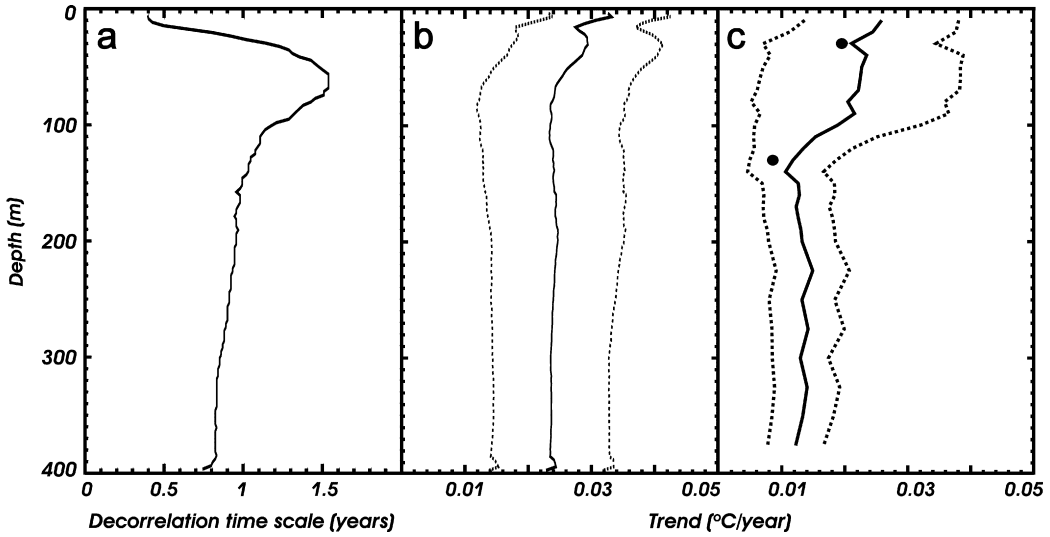

Fig. 5. (a) Decorrelation time scale at the Nanoose station determined according to Eq. (1). Panels (b) and (c) give the linear temperature trend in the central Strait of Georgia and offshore of Vancouver Island, respectively, for the period 1970–2005. Dotted lines indicate the 95% confidence intervals. The two dots in (c) indicate trends in average Line-P temperatures for the 10–50 and 100–150 m depth intervals.

2.1. Linear trends

Before giving further consideration to the detrended anomalies, it is appropriate to discuss the secular trends in temperature observed over the period 1970–2005. The depth-dependent linear trend is presented in Fig. 5b, along with 95% confidence limits determined using a standard t-test (e.g., Emery and Thomson, 2001). These confidence limits are based on an estimate of the equivalent sample size, $N = T/\tau_d$, where T is the record length (36 years) and the variation in the decorrelation time scale, τ_d, is shown in Fig. 5a. The estimated trends are significantly greater than zero through the entire water column. The magnitude of the secular trend increases somewhat approaching the surface, reaching a maximum value of $0.033\,^{\circ}\mathrm{C\,yr^{-1}}$ at a depth of 4.5 m. Below the surface, the temperature anomalies have a relatively constant trend, with magnitudes close to that of the depth-averaged anomalies. The latter have a trend of $0.024\,^{\circ}\mathrm{C\,yr^{-1}}$ with a 95% confidence interval of $\pm 0.01\,^{\circ}\mathrm{C\,yr^{-1}}$ based on a decorrelation time scale of 12.8 months and an equivalent sample size of 34.

The warming trend near the ocean surface at the Nanoose station may be expected to reflect the local air temperature trend over the same period. To verify this, monthly mean temperatures measured at four local meteorological stations were examined (see Fig. 1 for locations). For the study period 1970–2005, surface air temperatures increased at a rate of about $0.04\,^{\circ}\mathrm{C\,yr^{-1}}$ at all four meteorological stations, marginally higher than the rate found near the surface in the Strait. Similar trends in sea surface and air temperature have been observed over this period at other sites (e.g., Nixon et al., 2004).

It is interesting to compare the warming found within the Strait to the temperature trend seen over the same period at corresponding depths in the adjoining open ocean. For this purpose, a set of 7800 vertical profiles from an offshore region over the continental shelf and slope (Fig. 1) was assembled from CTD and bottle cast data drawn from the data archive at the Institute of Ocean Sciences. These profiles were averaged to form a set of quarterly 10–400 m temperature profiles with a vertical resolution of 10 (25) m above (below) 200 m depth. The few short gaps in the quarterly data have little influence on the computed linear trends. Results presented in Fig. 5c indicate that, over the study period, open ocean temperatures off Vancouver Island also have been rising at all depths over the upper 400 m of the water column. However, these trends show a larger vertical variation than in the Strait of Georgia. Within the upper 100 m of the water column, offshore temperatures have increased at approximately the same rate as within the Strait. Conversely, over the 100–400 m depth range, trends

in the Strait of Georgia are larger than those observed at comparable depths offshore by a factor of about two.

This difference is likely a consequence of the presence of the sills that restrict the exchange with offshore waters below 100 m depth, maintaining a lower seawater density within the Strait in comparison with water at similar depths offshore. Thus, the estuarine return flow can replenish the deep layers in the Strait with shelf water that originates from higher in the water column. Moreover, the return flow is modified through tidal mixing with near-surface water over shallow topography during its passage into the Strait. As a consequence, the warming seen at depth in the Strait reflects more closely regional trends occurring closer to the surface and is amplified in comparison to trends seen at similar depths over the offshore region.

2.2. Relation to atmospheric variability

In the seasonal cycle (Fig. 2), the near-surface layer varies, as expected, under the direct influence of local surface heat flux. We now consider the relation between the interannual variability of subsurface temperatures in the Strait and surface air temperatures. Semi-monthly air temperatures were formed from the daily mean temperatures measured at Victoria, British Columbia. Air temperature anomalies were obtained by removing the mean seasonal cycle and linear trend, and applying twice a 2.5 month boxcar filter. These anomalies have comparatively large spatial scales and similar results are obtained using data from the other meteorological stations indicated in Fig. 1. The lagged cross-correlation between the air temperature anomalies and the anomalies from the Nanoose station was determined for each 3 m depth bin below the surface. The resulting maximum correlation coefficient and corresponding optimal time lag at each depth are given in Fig. 6. The correlation coefficient decreases rapidly from values of about 0.62 near the surface to a minimum of about 0.36 around 30 m depth. A sub-surface maximum of about 0.64 is attained at around 100 m depth, within the core of the mid-depth intrusion layer (cf. Figs. 2 and 3). The higher correlation coefficient and shorter decorrelation time scale (Fig. 5a) at sill depth appears to reflect a more direct connection with the atmosphere for this layer, likely through the entrainment of surface layer anomalies within the subsurface estuarine return flow. Below the intrusion layer, the correlation with the surface decreases gradually to a value of approximately 0.55 in the deep basin.

The variation with depth of the maximum cross-correlation coefficient is associated with corresponding changes in the optimal time lag.

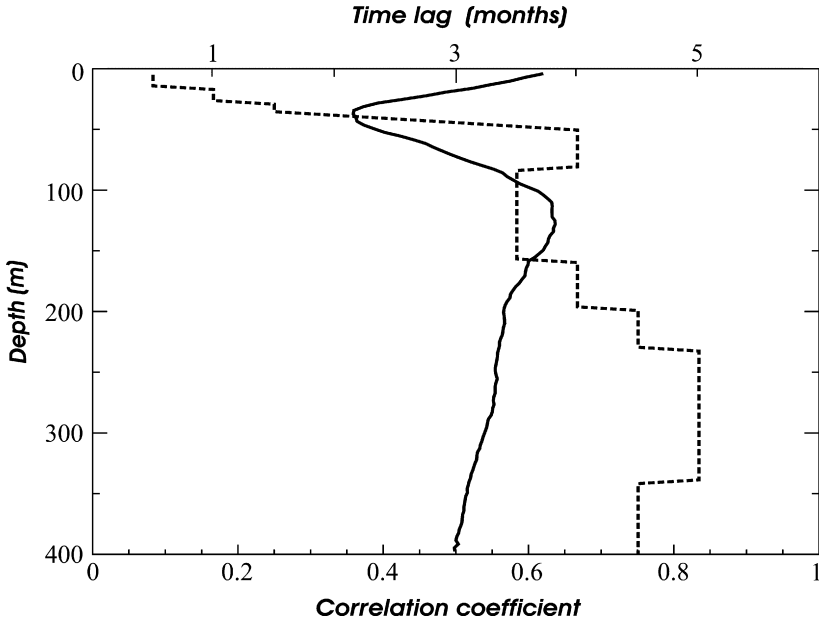

Fig. 6. Correlation coefficient (solid line) and optimal time lag (dashed line) between sub-surface temperature anomalies at the Nanoose station and semi-monthly air temperature anomalies measured at Victoria airport.

The variation in these lags is also shown in Fig. 6 and has a few local minima. The first is found near the surface where ocean temperatures lag by 0.5 month (the time increment). There is a strong gradient immediately below the surface layer and the optimal lag reaches a maximum of 4 months centered at a depth of 60 m. This maximum nearly coincides with the depth at which the variability has the lowest correlation with surface air temperatures and the longest integral time scale (Fig. 5a). A second minimum of 3.5 months in the optimal lag occurs within the depth range of the intrusion layer. This lag minimum is associated with a local maximum in the correlation with the surface air temperature. Below the intrusion layer the optimal lag gradually increases with depth to a maximum

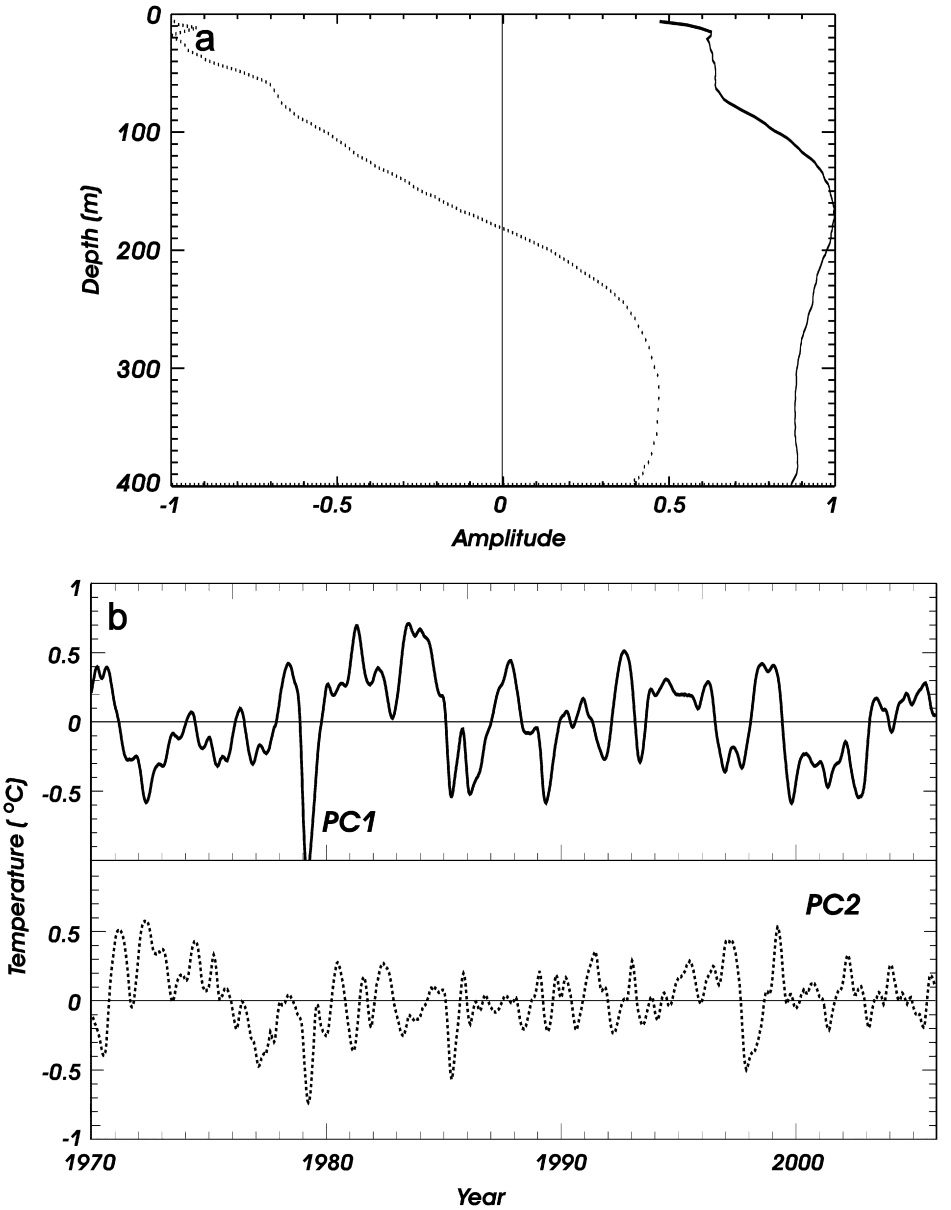

Fig. 7. EOFs (top panel) and associated principal components (middle and lower panel) of the first two modes of the detrended temperature anomalies at the Nanoose station. The EOFs are normalized to have a maximum absolute value of 1. The first EOF and its principal component (PC1) are indicated with solid lines; the second mode is shown with dotted lines.

value of 5 months. This increase may be associated with vertical diffusion and the mixing of anomalies carried by the intrusions.

To examine further the dominant variability and its vertical structure, the detrended temperature anomalies were expanded in terms of empirical orthogonal functions (EOFs). The two leading EOFs and their associated temporal amplitudes (the principal components) are given in Fig. 7. The first and second modes account for 78% and 13% of the variance, respectively. The first EOF represents in-phase variations through the water column and the principal component of this mode (hereinafter referred to as PC1) is very highly correlated with the depth-averaged anomalies. The amplitude of this mode (Fig. 7a) has a minimum near the surface and reaches its maximum value at a depth of about 170 m, between the level of the sill-depth intrusions and the deep basin. Over the lower half of the water column, the amplitude of the first mode decreases only slightly from its maximum value. The second mode, on the other hand, is surface intensified and its principal component fluctuates more rapidly than that of the first mode (Fig. 7b). This is reflected by the difference in the decorrelation time scales which is 12.8 months for PC1, compared with only 9.5 months for PC2. These results are also consistent with the expectation that higher frequency variability is more significant in the layer near the surface which is influenced most directly by atmospheric forcing.

The time series of semi-monthly air temperature anomalies measured at Victoria is plotted against PC1 in Fig. 8a, with both time series normalized by their standard deviations. As the unfiltered air temperature time series (not shown) displays

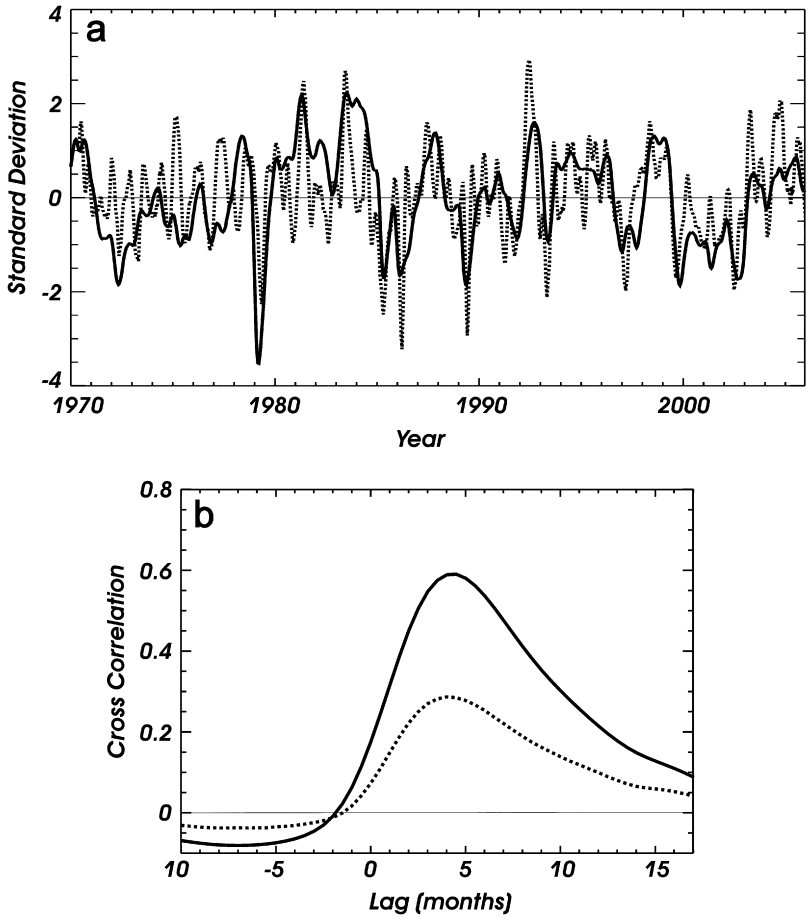

Fig. 8. (a) PC1 (solid line) and air temperature anomalies measured at Victoria (dotted line). The air temperature time series has been smoothed twice with a 2.5 month boxcar filter and advanced by 4.5 months. (b) Cross-correlation between the two time series (solid line) with air temperature anomalies leading for positive lags. The cross-correlation with unfiltered air temperature anomalies is also included (dotted line).

considerable high frequency variability, it has been smoothed twice with a 2.5 month boxcar filter. Fig. 8b shows that the maximum cross-correlation between PC1 and the smoothed air temperature anomalies ($r = 0.59$) occurs with the air temperature record advanced by 4.5 months, consistent with the results of Fig. 6. The non-zero values of the cross-correlation at zero and negative lags (ocean leading) are an artefact of the smoothing of the air temperature anomalies and are largely eliminated if the smoothing is omitted (cf. dotted curve in Fig. 8b).

Surface air temperature anomalies vary on large scales and may be assumed to correlate with surface heat flux and wind stress anomalies of similar scale. The structure of the cross-correlation functions in Fig. 8b suggest a cause-and-effect relationship where PC1, the dominant interannual signal observed in the Strait of Georgia, occurs in response to forcing by large scale atmospheric anomalies. The ocean signal apparently reflects the integrated influence of the atmospheric variability with the ocean acting as a low pass filter on the atmospheric forcing (e.g., Davis, 1976; Frankignoul, 1985). Similarly, Di Lorenzo et al. (2005) found that upper ocean temperature changes off southern California were driven primarily by spatially coherent changes in the net surface heat flux over the northeast Pacific.

PC1 was also compared with the monthly Bakun upwelling index at 125° W, 48° N, with varying degrees of smoothing applied to the index. Overall, the results (not shown) indicated a relatively weak relationship between the upwelling index and PC1. (A notable exception to this is the event discussed in Section 4.) For example, with the Bakun index smoothed twice with a 3 month boxcar filter, the maximum correlation, at a lag of 5 months, is 0.31, which is barely significantly different than zero at the 95% confidence level.

The subsurface advection of temperature anomalies by the estuarine circulation is likely important for the interannual variability in the deep Strait of Georgia. Properties of the estuarine return flow into the Strait are formed through a mixture of the surface outflow and the deep inflow advected from the shelf through Juan de Fuca Strait (e.g., Masson, 2006). While the surface waters are in direct contact with the atmosphere, the deep return flow is isolated from it during its advection up the estuary. Thus, there are two routes by which temperature anomalies may penetrate the deep waters of the Strait. One is advection by the estuarine return flow of anomalies established some time earlier offshore, along the west coast of Vancouver Island. A second is the downward mixing of surface layer anomalies over the shallow sills and passages between Juan de Fuca Strait and the Strait of Georgia, followed by the injection of these anomalies through subsurface intrusions into the Strait of Georgia. Both of these mechanisms may contribute to forming the deep anomalies and it is difficult to determine whether one generally dominates over the other. However, as discussed below, it is evident that at least for certain interannual events, such as the 1997/1998 El Niño, the advection of temperature anomalies from the offshore region is significant.

3. Co-variability at basin scale

The relation between the dominant variability in the central Strait of Georgia and the oceanic variability observed over the northeast Pacific is now considered. As it accounts for such a large fraction of the variance, PC1, the leading principal component, is taken as an index to represent the subsurface temperature variability in the Strait. The lighthouse time series at Amphitrite Point located on the west coast of Vancouver Island (Fig. 1) provides a useful measure of upper ocean temperature variability over the continental shelf. Freeland (1990) showed that SSTs at offshore BC lighthouses vary coherently with northern hemisphere air temperature anomalies over periods of 15 months to 4 years.

Fig. 9 compares PC1 with detrended SST anomalies from Amphitrite Point. In accordance

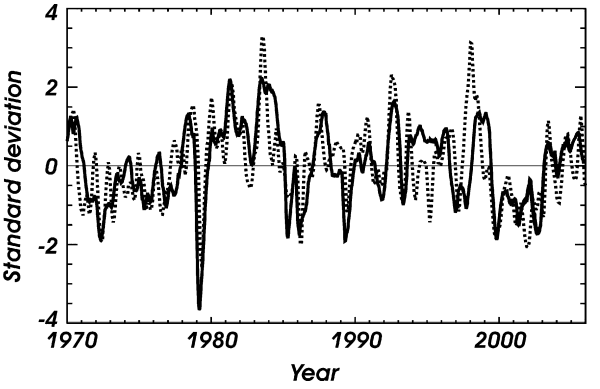

Fig. 9. PC1 (solid line) and SST (dotted line) measured at the Amphitrite Point lighthouse. The lighthouse time series has been smoothed twice with a 3 month boxcar filter and advanced by 4 months.

with the cross-correlation function (not shown), the lighthouse data were advanced by 4 months in Fig. 9 to optimize the correlation with PC1 ($r = 0.64$). The two time series in Fig. 9 have most large peaks in common and it is evident that the variability within the Strait of Georgia reflects the offshore variability with a lag of a few months. The lag of 4 months is consistent with the lag found between the intrusion layer and surface air temperatures (Fig. 6). It is also comparable to the time lag seen in the seasonal cycle between the maximum in surface temperature and subsurface maxima occurring around sill depth (Fig. 2). Assuming a lag, τ, of 4 months and a travel distance, L, of 300 km between the coastal region near the mouth of Juan de Fuca and the central Strait yields a scale velocity, $U = L\tau^{-1}$, of about $3\,\mathrm{cm\,s^{-1}}$ for the advection of subsurface anomalies between the shelf and the Nanoose station. The deep estuarine return flow readily supports such a speed (e.g., Ott et al., 2002; Masson and Cummins, 2004). Thus, the time lag obtained between variability off the west coast of Vancouver Island and the subsurface variability in the central Strait is sufficiently long to be accounted for by the advection of offshore anomalies by the estuarine inflow.

In Fig. 9, a notable discrepancy between PC1 and the lighthouse time series occurs in 1997. The onset of tropical El Niño conditions led to a large increase in temperature at the lighthouse station in early 1997. This event was followed by a warming in the central Strait, but with a delay of 10 rather than 4 months relative to the lighthouse temperatures. The reason for the early warming in the lighthouse data is the development in the late summer of 1997 of a superficial surface layer (<50 m thick) of positive temperature anomalies over the Gulf of Alaska (e.g., Royer, 2005). This warming is thought to have arisen due to an atmospheric teleconnection driven by equatorial SST anomalies (Overland et al., 2001). The warm surface layer is evident in the cross-section of temperature anomalies along Line-P presented in Fig. 4c of Freeland (2002). However, this early warming was not manifested in the deep Strait of Georgia. By February, 1998 a 100 km wide lens of warm water extending down to 400 m depth had developed adjacent to the coast (Fig. 4e of Freeland, 2002), presumably due to anomalous northward advection along the coastal wave guide. The presence of this water mass was then followed, about 4 months later, by a warming in the central Strait of Georgia, as represented in PC1. In this regard, the response of the northeast Pacific associated with the 1997/1998 El Niño differs from that of the major El Niño of 1982/1983. A similar thick lens of warm water developed adjacent to the coast in March, 1983 (Freeland and Thomson, 1999) which was also followed 3–4 months later by a signal in the central Strait. However, in contrast to the 1997/1998 event, the warm pulse adjacent to the coast was not preceded by a basin-wide superficial warming over the Gulf of Alaska.

PC1 is now compared with observations from Line-P to examine its relation to the variability occurring at basin scales over the northeast Pacific. Stations along Line-P have been occupied regularly since the 1950s, with the 13 original stations expanded to 27 stations in the 1960s. For each station, time series of annual summer (JAS) and winter (JFM) temperatures averaged over the depth intervals 10–50 and 100–150 m were constructed by Dr. W. Crawford (pers. comm.). The former depth interval is within the layer directly influenced by the surface heat flux and includes the seasonal thermocline, whereas the deeper interval encompasses the main pycnocline. There are just a few gaps in the summer data, however the sampling is appreciably poorer for the winter data. (A Hovmøller diagram of the 100–150 m summer data is presented in Crawford et al., 2005.) To simplify the comparison and also to mitigate the problem of data gaps, the Line-P anomalies for each station were averaged together to form a single time series for each of the two depth intervals. The averaging gives equal weight to all the stations along the line, except for the one that is closest to the west coast of Vancouver Island which is omitted. The latter is representative of conditions over the inner shelf and, in fact, corresponds closely to the temperature record from the Amphitrite Point lighthouse (Fig. 9).

Linear trends for the period 1970–2004 were removed from the average 10–50 and 100–150 m Line-P anomalies, and each time series was normalized by its standard deviation. (As indicated in Fig. 5c, the magnitude of these trends is consistent with those found at comparable depths in the composite profiles for the region off Vancouver Island.) Fig. 10 compares PC1 with the average detrended Line-P temperature anomalies for the 10–50 and 100–150 m depth intervals. To improve the visual correspondence with PC1, the Line-P time series for the 10–50 m anomalies was advanced by half a year, while the 100–150 m time series was

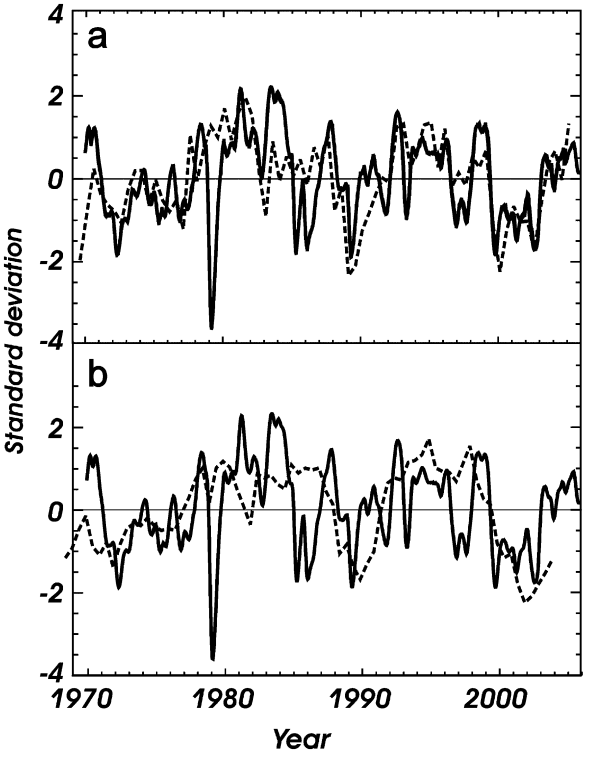

Fig. 10. Comparison between PC1 (solid lines) and average temperature anomalies along Line-P (dashed lines) for (a) the 10–50 m, and (b) 100–150 m depth intervals. The Line-P time series were detrended and normalized by their standard deviations. In (a), the Line-P time series is advanced by 6 months, while in (b) it is delayed by 1 year.

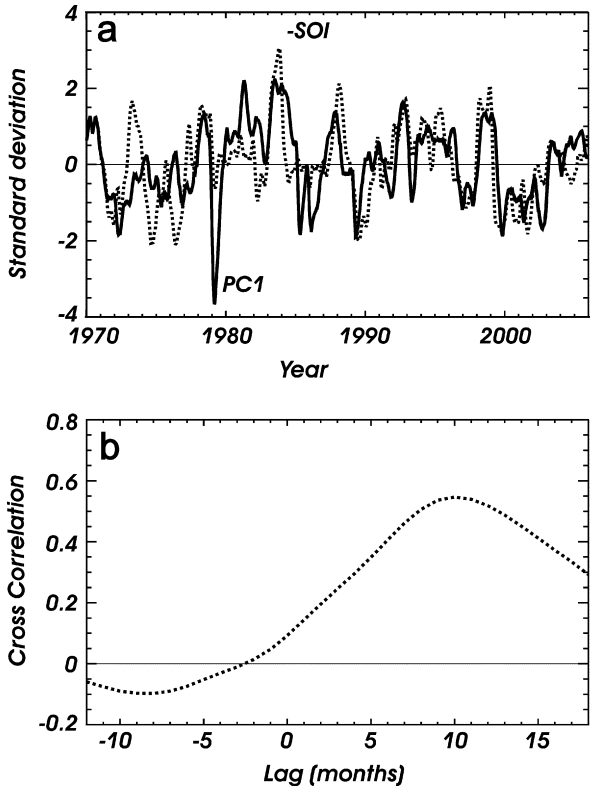

Fig. 11. (a) Comparison between PC1 and monthly values of the negative of the Southern Oscillation Index (–SOI). The latter was smoothed twice with a 3 month boxcar filter and advanced by 10 months relative to PC1. Both time series were normalized by their standard deviations over the period 1970–2005. (b) Cross-correlation between –SOI and PC1 with –SOI leading for positive lags.

delayed by 1 year. The results of Fig. 10a show that except for a few events in PC1, most notably the cold anomaly of winter 1978/1979 and also the positive anomaly of 1983, there is generally good agreement between temperatures in the central Strait and the average 10–50 m temperatures along Line-P. This is consistent with the results discussed above and indicates that temperature anomalies through the water column in the Strait of Georgia tend to co-vary with the near-surface temperature variability over the northeast Pacific. There appears to be a time lag of about 4–6 months for the response within Strait. However, given the semi-annual resolution of the Line-P anomalies, it is not possible to establish the optimal lag more precisely. The results of Fig. 10a are consistent with the view that large scale atmospheric forcing is the common driving mechanism for these anomalies.

On the other hand, temperature anomalies at 100–150 m depth along Line-P compare less favourably with PC1, although there is some correspondence between the time series at decadal periods. Line-P anomalies at this depth interval are dominated by low frequency variability and changes on interannual time scales are less prominent than in PC1 or the 10–50 m temperature time series. Wind forcing, in particular anomalous Ekman pumping, plays an important role in driving long period variability in the depth of the pycnocline at Station P (Cummins and Lagerloef, 2002). This may be expected also to be an important driving mechanism for the 100–150 m anomalies and perhaps also for the low frequency modulation of temperatures in the Strait of Georgia.

PC1 also appears to be related to a global scale climate index. Fig. 11 compares PC1 with the negative of the Southern Oscillation Index (SOI), defined as the difference between monthly mean sea level pressure anomalies at Tahiti and Darwin

(Trenberth, 1984). Here the index has been advanced by 10 months to optimize the correspondence with PC1. Fig. 11 shows a rather close relationship between PC1 and the SOI, particularly after 1980, and there is an obvious correspondence between several prominent peaks in the two time series. This includes the maxima and minima seen in PC1 that are associated with major El Niño and La Niña events. In addition, the signature of the recent cool period of 1999–2002 following the 1998/1999 La Niña (Peterson and Schwing, 2003; Cummins et al., 2005) is evident. (This is also seen in the 10–50 m Line-P anomalies of Fig. 10a.) There are also notable discrepancies between the two time series. Once again, the most prominent one is associated with the 1978/1979 cold event. However, there is also a pair of less extreme cold events for 1985 and 1986 which also do not correspond to events in the SOI time series. In addition, the 1972 El Niño event is not reflected in PC1. This is consistent with the results of Freeland (1990) who found that no signal associated with the 1972 El Niño was evident in British Columbia lighthouse data.

The relationship between PC1 and the Pacific Decadal Oscillation (PDO) Index also has been examined. However, the results are not shown as the correlation of PC1 with the PDO is appreciably weaker than with the SOI. This reflects the fact that PC1, like the SOI, is dominated by interannual events, whereas lower frequency, interdecadal variability dominates the PDO record (e.g., Zhang et al., 1997).

4. The cold intrusion of winter 1978/1979

The pronounced negative sub-surface temperature anomaly recorded in the winter of 1978/1979 is one of the most remarkable events in the time series of interannual anomalies at the Nanoose station. The signature of this event is clearly evident over most of the water column (Fig. 4a, b), although its expression is muted near the surface. The event is reflected in PC1 (Fig. 7), where it appears as the single strongest signal over the entire 36 year record with an amplitude of nearly 4 standard deviations. There is evidence that the cold event in the Strait of Georgia was preceded by a significant anomaly at the Amphitrite Point lighthouse station (Fig. 9). However, the anomaly is not manifested much beyond the continental shelf along Line-P (Fig. 10).

The cold event of winter 1978/1979 appears to have resulted from a combination of local factors.

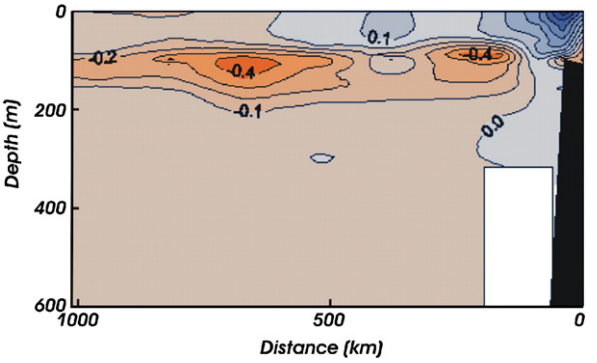

Fig. 12. Density (σ_t) anomalies along Line-P for January, 1979. The anomalies were computed relative to the climatological seasonal cycle for the period 1956–1991 and are contoured at intervals of 0.1 kg m^{-3}.

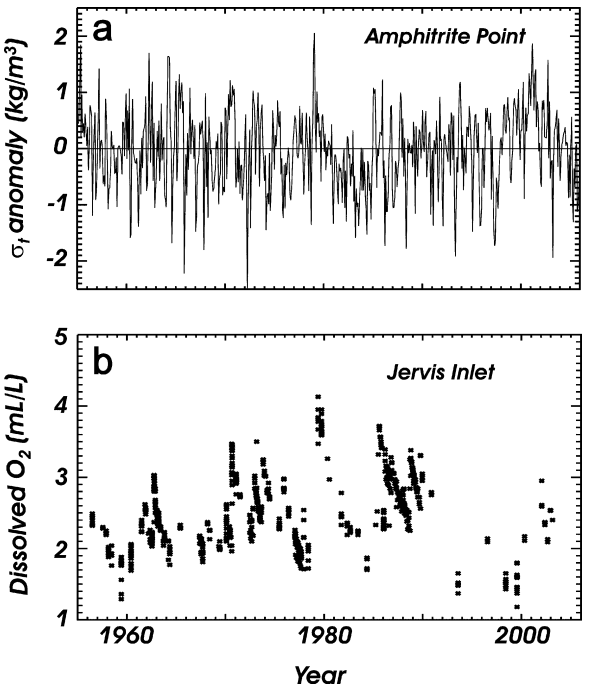

Fig. 13. (a) Monthly density anomalies at the Amphitrite Point lighthouse relative to the climatology seasonal cycle for the period 1935–2005. (b) Time series of dissolved oxygen in the deep waters of Jervis Inlet. Locations are indicated in Fig. 1.

Firstly, a cold front passed over the coastal area, producing low air temperatures and dry conditions. At the same time, there was a period of sustained upwelling winds, which is unusual during the winter along the west coast of Vancouver Island. The response to these forcings was the development of a lens of cold, saline (hence dense) water on the shelf. The presence of this anomalous water mass is

evident in the Line-P section from January, 1979 (Fig. 12) which shows the occurrence of highly anomalously dense water confined to within 100 km of the coast. Further offshore, salinity and temperature anomalies were mostly of opposite sign.

The density of sea water sampled at the Amphitrite lighthouse (Fig. 13a) reached in January, 1979 its highest monthly mean value since sampling began in 1934. High salinities had the dominant effect on the density anomaly, although the low temperatures contributed somewhat as well. The cold saline water mass found offshore entered Juan de Fuca Strait with the deep estuarine return flow. The resulting mixing with the cold surface waters produced water sufficiently dense to penetrate the deep Strait of Georgia as a very cold subsurface water mass. These dense intrusions then filled the deep coastal basin in the early winter, a time of year when deep water renewal does not usually occur (Masson, 2002). This resulted in the marked low temperature anomalies recorded at the Nanoose station.

The signature of this unusual winter intrusion is also evident in time series at other nearby locations and in different water properties. For example, temperatures in the deep (400–600 m) basin of Jervis Inlet, a long deep fjord adjoining the Strait of Georgia (Fig. 1), reached their lowest recorded values in early 1979. As seen in Fig. 13b, the deep waters of Jervis Inlet are subject to interannual flushing events which raise substantially the concentration of dissolved oxygen. The 1978/1979 intrusion produced the highest values of dissolved oxygen recorded in the deep basin of Jervis Inlet.

While the 1978/1979 cold intrusion was particularly intense, the Nanoose data suggest that other less extreme cold events of local origin also occurred in 1985 and 1986. In this regard, we note that the negative extrema in PC1 during these years correspond to negative temperature anomalies observed in local air temperature (Fig. 8a) and SST at Amphitrite Point (Fig. 9). Moreover, these events have no signature in the Line-P record (Fig. 10), or in the SOI (Fig. 11). These characteristics are consistent with those of the 1978/1979 event and suggest the occurrence of interannual variability at local rather than basin scale.

5. Summary

We have examined the interannual and secular variability of temperature through the water column in the central Strait of Georgia in terms of a continuous time series of semi-monthly vertical temperature profiles extending over a 36 year period (1970–2005). In addition to seasonal changes, these data clearly show pronounced interannual events and secular trends. With respect to the seasonal variability, the data disclose the three-layer structure of the water column with a relatively thin surface layer directly influenced by surface heat fluxes, a mid-water layer centered around sill depth (100 m) subject to frequent intrusions driven by the estuarine circulation, and the deep layer that is partially isolated from the open ocean by the presence of shallow sills.

Near surface and deep temperatures from the Nanoose station are well correlated with large-scale surface air temperature anomalies, at lags of 0.5 month and 4.5 months, respectively. The 0.5 month lag indicates a relatively short time scale adjustment between the surface waters and the overlying atmosphere. On the other hand, the longer lag for subsurface temperature anomalies is likely associated with a transport mechanism involving a combination of the advection of temperature anomalies from the shelf by the deep estuarine inflow and tidal mixing in Haro Strait of surface layer anomalies into the deep flow inflow.

An EOF analysis of the profiles yields a dominant first mode representing some 78% of the variance. The principal component of this mode (PC1) has a decorrelation time scale of 12.8 months and accurately represents the dominant interannual variability for most of the water column, particularly below 100 m depth. Accordingly, it is used as an index of variability in the Strait of Georgia.

PC1 was compared with SST anomalies from the Amphitrite Point lighthouse on the west coast of Vancouver Island, and with observations taken along Line-P, an oceanographic section extending from the BC coast to Ocean Weather Station P in the subarctic N. Pacific. The results show a marked co-variability of PC1 with large scale, upper ocean temperatures over the northeast Pacific with a lag of about 4 months. This suggests that large scale atmospheric variability over the region, including anomalous wind stresses (Ekman pumping) and surface heat fluxes, are the primary forcing for the temperature variability through water column in the Strait of Georgia.

There are significant anomalies that are linked to coastal ocean processes. For example, following tropical El Niño events, positive temperature

anomalies occurred in the Strait in 1983 and 1998 that are associated with the presence of coastally trapped lenses of warm water. These likely developed due to lateral advection by anomalous currents along the coastal ocean wave guide. Particular attention has been given to the negative anomaly observed during the winter of 1978/1979, which is the single largest event (>3.5 standard deviations) seen in PC1. This extreme event appears to have been produced by the simultaneous occurrence of anomalously cold and dry local weather, combined with an unusual period of sustained upwelling winds offshore. These local conditions appear to have produced a major deep water renewal event during winter, a time of year when such events do not normally occur.

A comparison of PC1 with the SOI shows a relation between variability in the tropical Pacific and the local coastal variability with a lag of 10 months. The 10 month lag of the temperature response of the Strait relative to the SOI offers, to some degree, the potential of predictability which could possibly be exploited, for example in the management of local fisheries.

Over the 400 m depth of the water column, vertically averaged temperatures in the central Strait of Georgia have been increasing at a rate of $0.024 \pm 0.01\,^{\circ}\mathrm{C\,yr^{-1}}$. This rate is comparable to the warming observed offshore near the surface, but exceeds, by a factor of at least two, the rate of warming measured offshore below 100 m. The enhanced rate of warming observed in the subsurface Strait is likely a consequence of transport mechanisms associated with the estuarine circulation. Mid-depth intrusions and deep water renewal events provide a mechanism for the subduction of near-surface thermal anomalies into the deep basin. The amplified response seen at depth in the Strait compared with offshore regions is indicative of the special vulnerability of coastal basins, and the ecosystems that they support, to the impact of global climatic changes.

Acknowledgements

Bill Crawford kindly provided the Line-P temperature data. We thank Ron Perkin for providing the data from the Nanoose station, Dario Stucchi for the oxygen data from Jervis Inlet, and Marie Robert for the figure of Line-P density anomalies. We are also grateful to Howard Freeland and Rick Thomson for discussions. Some of the figures were prepared with ODV software (Schlitzer, 2002).

Appendix A

Data from the Nanoose station have been collected with the primary objective of determining vertical variations in sound speed within the water column. Details of measurement techniques and quality controls have been discussed by Fissel et al. (1991). They note that because it is critical in determining the sound velocity, temperature has been measured consistently to within an accuracy of $\pm 0.1\,^{\circ}\mathrm{C}$ or better. Improved measurement and recording systems have been implemented over the course of the time series. Initially (1970–1979), temperature was measured with a platinum resistance thermistor (instrument accurate to $\pm 0.02\,^{\circ}\mathrm{C}$) as part of a sound-speed, temperature and pressure recorder (STVP). In 1979, the STVP system was replaced by a Neil Brown CTD. Finally, a Seabird CTD system has been in use since 1996. Both CTDs are accurate to $\pm 0.005\,^{\circ}\mathrm{C}$.

References

Crawford, W., Sutherland, P., van Hardenberg, P., 2005. Cold water intrusion in the eastern Gulf of Alaska in 2002. Atmosphere-Ocean 43, 119–128.

Cummins, P.F., Lagerloef, G.S.E., 2002. Low frequency pycnocline depth variability at Ocean Weather Station P in the northeast Pacific. Journal of Physical Oceanography 32, 3207–3215.

Cummins, P.F., Lagerloef, G.S.E., Mitchum, G., 2005. A regional index of northeast Pacific variability based on satellite altimeter data. Geophysical Research Letters 32, L17607.

Davis, R.E., 1976. Predictability of sea surface temperature and sea level pressure anomalies over the North Pacific Ocean. Journal of Physical Oceanography 6, 249–266.

Di Lorenzo, E., Miller, A.J., Schneider, N., McWilliams, J.C., 2005. The warming of the California current system: dynamics and ecosystem implications. Journal of Physical Oceanography 35, 336–362.

Emery, W.J., Thomson, R.E., 2001. Data Analysis Methods in Physical Oceanography, second ed. Elsevier, Amsterdam.

Fissel, D.B., Birch, J.R., Chave, R.A.J., 1991. Measurements of temperature, salinity, and sound velocity at the Nanoose Bay Naval Underwater Weapons Test Range, 1967–1984. Report prepared by Arctic Sciences Ltd., Sidney, BC.

Frankignoul, C., 1985. Sea surface temperature anomalies, planetary waves, and air-sea feedback in the middle latitudes. Reviews of Geophysics 23 (4), 357–390.

Freeland, H.J., 1990. Sea surface temperatures along the coast of British Columbia: regional evidence of a warming trend. Canadian Journal of Fisheries and Aquatic Sciences 47, 346–350.

Freeland, H.J., 2002. The heat flux across Line-P 1996–1999. Atmosphere-Ocean 40, 81–89.

Freeland, H.J., Thomson, R.E., 1999. The El Niño signal along the west coast of Canada—temperature, salinity and velocity. In: PICES Scientific Report No. 10, Sidney, BC, pp. 55–58.

Gower, J.F.R., 2002. Temperature, wind, wave climatologies, and trends from marine meteorological buoys in the Northeast Pacific. Journal of Climate 15, 3709–3718.

LeBlond, P.H., 1983. The Strait of Georgia: functional anatomy of a coastal sea. Canadian Journal of Fisheries and Aquatic Sciences 40, 1033–1063.

Masson, D., 2002. Deep water renewal in the Strait of Georgia. Estuarine, Coastal and Shelf Science 54, 115–126.

Masson, D., 2006. Seasonal water mass analysis for the Straits of Juan de Fuca and Georgia. Atmosphere-Ocean 44, 1–15.

Masson, D., Cummins, P.F., 2004. Observations and modeling of seasonal variability in the Straits of Georgia and Juan de Fuca. Journal of Marine Research 62, 491–516.

Nixon, S.W., Granger, S., Buckley, B.A., Lamont, M., Rowell, B., 2004. A one hundred and seventeen year coastal water temperature record for Woods Hole, Massachusetts. Estuaries 27, 397–404.

Ott, M.W., Dewey, R., Garrett, C., 2002. Reynolds stresses and secondary circulation in a stratified rotating shear flow. Journal of Physical Oceanography 32, 3249–3268.

Overland, J.E., Bond, N.A., Adams, J.M., 2001. North Pacific atmospheric and SST anomalies in 1997: links to El Niño? Fisheries Oceanography 10, 69–80.

Peterson, W.T., Schwing, F.B., 2003. A new climate regime in northeast Pacific ecosystems. Geophysical Research Letters 30 (17), 1896.

Pickard, G.L., 1975. Annual and longer-term variations of deepwater properties in the coastal waters of southern British Columbia. Journal of the Fisheries Research Board of Canada 32, 1561–1587.

Royer, T.C., 2005. Hydrographic responses at a costal site in the northern Gulf of Alaska to seasonal and Interannual forcing. Deep Sea Research II 52, 267–288.

Schlitzer, R., 2002. Ocean Data View, ⟨http://www.awi-bremerhaven.de/GEO/ODV⟩.

Trenberth, K.E., 1984. Signal versus noise in the Southern Oscillation. Monthly Weather Review 112, 326–332.

von Storch, H., Zwiers, F.W., 1999. Statistical Analysis in Climate Research. Cambridge University Press, Cambridge, UK.

Waldichuk, M., 1957. Physical oceanography of the Strait of Georgia, British Columbia. Journal of the Fisheries Research Board of Canada 14, 321–486.

Zhang, Y., Wallace, J.M., Battisti, D.S., 1997. ENSO-like interdecadal variability: 1900–93. Journal of Climate 10, 1004–1020.